Coupled Systems Mechanics, *Vol. 12, No. 6 (2023) 481-501*
https://doi.org/10.12989/csm.2023.12.6.481

Numerical formulation solid-layer finite element to simulate reinforced concrete structures strengthened by over-coating

Arturo Suárez-Suárez*[1], Norberto Domínguez-Ramírez[2a] and Orlando Susarrey-Huerta[1b]

[1]*Postgraduate Studies and Research Section, ESIME-UZ, Instituto Politécnico Nacional, Mexico*
[2]*Postgraduate Studies and Research Section, ESIA-UZ, Instituto Politécnico Nacional, Mexico*

(Received March 31, 2023, Revised November 16, 2023, Accepted November 16, 2023)

Abstract. Over-coating is one of the most popular engineering practices to strengthen Reinforced Concrete (RC) structures, due to the relative quickness and ease of construction. It consists of an external coat bonded to the outer surface of the structural RC element, either by the use of chemical adhesives, mechanical anchor bolts or simply mortar injection. In contrast to these constructive advantages, the numerical estimation of the bearing capacity of the strengthened reinforced concrete element is still complicated, not only for the complexity of modelling a flexible membrane or plate attached to a quasi-rigid solid, but also for the difficulties that raise of simulating any potential delamination between both materials. For these reasons, the standard engineering calculations used in the practice remain very approximated and clumsy. In this work, we propose the formulation of a new 2D solid-layer finite element capable to link a solid body with a flexible thin layer, as it were the "skin" of the body, allowing the potential delamination between both materials. In numerical terms, this "skin" element is intended to work as a transitional region between a solid body (modelled with a classical formulation of a standard quadrilateral four-nodes element) and a flexible coat layer (modelled with cubic beam element), dealing with the incompatibility of Degrees-Of-Freedom between them (two DOF for the solid and three DOF for the beam). The aim of the solid-layer element is to simplify the mesh construction of the strengthened RC element being aware of two aspects: a) to prevent the inappropriate use of very small solid elements to simulate the coat; b) to improve the numerical estimation of the real bearing capacity of the strengthened element when the coat is attached or detached from the solid body.

Keywords: delamination; finite element formulation; solid-layer bonding

1. Introduction

Reinforced Concrete (RC) has been the most used material to construct a large amount of buildings and facilities, since its invention in the XIXth Century, promoting the economical and social development of many countries. Unfortunately, Reinforced Concrete's integrity is susceptible to suffer long-term alterations, either by the local weather's effects (corrosion of steel)

*Corresponding author, Ph.D., E-mail: asuarezs@ipn.mx
[a]Professor, E-mail: ndominguez@ipn.mx
[b]Professor, E-mail: osusarrey@yahoo.com

http://www.techno-press.org/?journal=csm&subpage=8 ISSN: 2234-2184 (Print), 2234-2192 (Online)

or by the unexpected mechanical effects of extreme hazards (cracking in concrete after an earthquake), making it necessary to repair it promptly in order to recover the loading capacity of the affected RC element (Xiong and Yue 2019). There are also some other reasons to strengthen existing RC structures such as the refurbishing of an old building by a land-use change or the transformation of a conventional building in a new *Resilient Critical Structure*, as it is foreseen in the framework of the new *Resilience-Based Design*, whose philosophy is to preserve the functionality of critical buildings and facilities after any natural hazard occurs (Cimellaro 2013) (Matthew and Mehrdad 2019), or even when a vibration is induced in the concrete elements due to various artificial (Akbaş 2019, 2020). In either case, adding a new coat over the lateral surface of a RC element has been an excellent solution in terms of construction practices, abating time and procedure's complexity: whether they are pieces of the super structure or in foundations, it's always easier to reinforce them with a coat as proposed by (Rabahi *et al.* 2020). Likewise, the over-coating can be performed with steel plates (Siu *et al.* 2011), fiberglass or any other material (Bideci *et al.* 2017), bonded to the outer element faces through the use of chemical adhesives, mechanical anchor bolts or simply mortar injection (Iglesias *et al.* 1985, Mac Gregor *et al.* 1997, Yang *et al.* 2015). Once installed, coating must provide confinement, control of cracking and a quick increase of RC resistance, based on the assumption that both materials (the existing one and the new one) are working well together. However, the success of the reinforcement relies on several mechanical aspects, like the ability of the bonding to transfer the internal efforts between the coat and the existing RC element (Al-Osta 2019, Mehdi *et al.* 2021); the suppression of sliding and decohesion between both surfaces; the harnessing of the combined bearing capacity; etc. Therefore, one question raises: how to estimate the new capacity of the strengthened RC element considering all these aspects before proceeding to reinforce?

One possible answer could be to make some experimental tests accompanied by advanced numerical analysis (Shaw and Andrawes 2017). Unfortunately, not only these tasks become expensive and difficult to implement, but even worse, there are some physical issues related to the attachment/delamination phenomena that remains unsolved: if an engineer wants to study better the mixed behaviors of a reinforced element considering all these aspects through the construction of a finite element model, he will be confronted to the fact that there is not a specific finite element solution to simulate the physical problem of linking a rigid solid body with a flexible coat layer (Khandaker 2004, Mohebi *et al.* 2016, Daouadji 2017). For these reasons, most of the standard structural design codes prefer to recommend the use of simplified equations to estimate the bearing capacity of a strengthened RC element (CDMX 2017), instead of using complex numerical analysis (Pajand and Karimipour 2020). However, these simplified equations become inefficient for some cases as evaluating the real capacity of a damaged mixed structure after the occurrence of an earthquake, particularly if any delamination process has started between the concrete and the coat. In order to deal with all these lacks, it seems necessary to develop a robust numerical analysis of the mixed structure that includes the phenomenon of bonding/delamination between the concrete and the coat, taking care of the following issues:

- The combined capacity of the reinforced element depends on the non-linear nature of the three components (concrete, coat and bond) and how they are correlated. In other words, the stiffness of each component is related to its material properties as well as its geometrical shape, affecting the flexibility and the non-linear response of the entire system;
- Bonding between both materials is not perfect, so the integrity of the entire system cannot be guaranteed or prevented from deterioration along the time, inducing a sort of delamination between the coat and the concrete;

• The delamination phenomenon is an evolving process with at least four well-identified phases, where bonding can disappear completely in the last phase, allowing the coat behaves like a flexible body;
• The numerical modelling of the three components (RC element, coat and bond) could lead to the deployment of special non-linear techniques as well as the use of specific finite elements for each component, which might be mutually incompatible.

Prior to take on the development of a new numerical solution for over-coating and delamination of RC structures, some of the physical features of these phenomena will be reviewed in the following section.

1.1 Physical description of the delamination phenomenon

When over-coating is used, the bearing capacity of any strengthened RC element depends not only on the particular behavior of the concrete and the coat, but also on the effectiveness of the bonding, which relies on another mechanical phenomenon that should be taken into account: delamination. Physically, delamination or ex-foliation corresponds to the separation of two or more individual layers of a heterogeneous material (Park *et al.* 2007) induced by the combined action of normal and shear stresses, which simultaneously produce decohesion and sliding at the interface of such materials (Tahar *et al.* 2020, Tahar *et al.* 2021). This situation might lead to a certain type of local failure in the structural element, where the additional confinement provided by the coating disappears while the loss of effective area increases, engendering a local hinge inducing the collapse of the structural element (Lee *et al.* 2019). Some theoretical and experimental tests focused on delamination of reinforced compounds of polymer fiber have been carried out to achieve a better understanding of the physical origin of hardness in delamination fracture (Limaiem *et al.* 2019). Taking as starting point that the bearing capacity of a coated RC element relies on the delamination's progression, we can formulate the following hypothesis: *the behavior of the whole assembly mainly depends on the delamination mechanism's state and not only on each component's material behavior, being a function of the severity of bonding's damage*. Moreover, we can identify at least four phases during the progression of the delamination's phenomena:

Phase 1 Bonding between RC element and the coat is perfect, so there is no additional strain energy at the interface. Therefore, the coat adopts the same configuration of the solid without any decohesion or sliding. Nevertheless, at the very beginning of the process, one of these three configurations can be adopted by the assembly:

(a) The solid is very rigid and cannot develop any rotation on its surface, preventing any rotation on the coat.
(b) The solid is very flexible and its surface can rotate as well as the coat, which remains attached to the solid.
(c) The solid is very flexible but the coat is much stiffer, so the solid adopts the coat configuration.

Phase 2 Bonding between RC element and the coat can develop a pseudo-material elastic behavior, allowing small sliding or decohesion. The bonding interface plays a role in the total strain energy of the assembly.

Phase 3 As a certain yield point is reached at bonding, the coat could be partially detached from the rigid solid in some points, but it is still connected in other regions, some of them perfectly bonded. The coat might develop large rotations in some separated regions.

Phase 4 The coat is detached from the rigid solid in large regions, as soon as a pseudo-coalescence phenomenon occurs in different bonded points.

Some numerical works have tried to deal with the problem of delamination, most of them for flexible layers of composite structures -almost none for a solid-layer combination. Nevertheless, one of the most recent developments for a problem of this type is the solid-like shell (De Borst and Remmers 2006), which is a volume element for thin-layered composite structures that exploits the Partition-of-Unity Principle to simulate the crack at any arbitrary location inside. However, its performance is still limited due to some disadvantages, as the emergence of spurious elastic deformations prior to delamination onset occurs. As it can be constated, the major difficulty involves how to simulate a hard (or flexible) solid body attached to a flexible (or rigid) shell through the use of a bonding interface (Sang and Aboutaha 2004), governed by different laws of deformability, behaviour and equilibrium. A current suggestion is to model the quasi-rigid body as a 2D/3D solid element, while the coating can be simulated with trusses or thin plates. Unfortunately, both finite element formulations are numerically incompatible when they share the same nodal points. Needless to say, that problem becomes much more complicated if bonding is considered into the global modelling. One possibility is to use bond interface elements or enriched solid elements (Dominguez *et al.* 2010), but another difficulty that is necessary to mention is the variation of constitutive laws according to the corresponding phase of delamination. For all these drawbacks, we propose to develop a new dedicated finite element as it is explained in subsequent sections.

2. Mathematical formulation of the solid-layer element

2.1 Underlying assumptions.

The aim of the 2D solid-layer element introduced in this work, is to deal with the different kinematics and non-linear behavior of the three components (rigid reinforced concrete (RC), flexible coating and transitional bonding), evolving according to the state of the delamination phases described previously. The 2D solid-layer element (or *skin-element* as we called) is the combination of three finite element formulations: a classical four-node quadrilateral element, a Hermitian beam element and an interface element intended to solve the incompatibility of Degrees-of-Freedom between the solid formulation (two translational DOF by node) and the beam formulation (with a third rotational DOF), avoiding the use of very tiny quadrilateral elements to represent the coat, improving its real behavior in case to be detached from the solid. To illustrate how the solid-layer element functions, let's take the case of an orange peel: At the beginning, the peel covers the whole orange's internal body, attached through a set of tiny hairs forming a soft interface. As soon as an external loading is applied on the orange, the peel tries to separate from the orange's body. Nevertheless, there are some *"tiny hairs"* that keep attached the peel to the body avoiding its free movement. If the tiny hairs are cut in some regions, the peel is fully detached, and it could start rolling up according to the flexibility of the skin. The aim of the *"skin element"* is to reproduce these different responses during delamination process. For this very first approach, the skin element is still limited to reproduce only three phases (see Fig. 1):

- *"Phase 1: perfect bonding"*, taking into account two different body-coat relationships: rigid-body/flexible-coat and flexible-body/flexible-coat);
- *"Phase 2: elastic threshold delamination"*, defined by a simple yield point criterion; and

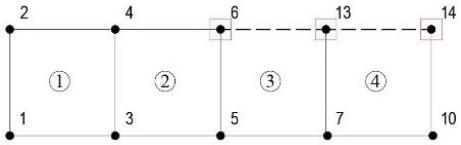

(a) Phase 1: Mesh of solid-layer elements with the coat fully attached

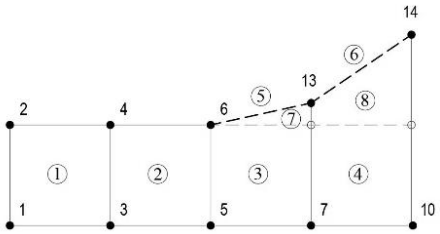

(b) Phase 2: Activation of the interface region to simulate coat's partial detachment from the solid element

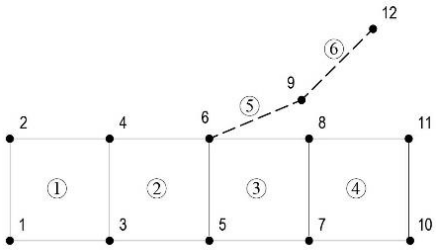

(c) Phase 3: Coating freely detached from the solid element

Fig. 1 Phases of the solid-layer element to reproduce joining and detachment of a flexible coat from a solid body, controlled by an internal interface element

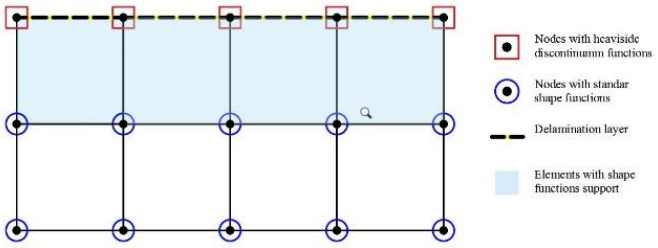

Fig. 2 Mesh construction coupling standard finite elements with solid-layer elements

•*"Phase 3: partial detachment"*, simulating detachment in some points of the mesh, as it is described later in the following sections.

Since the point of view of a practical construction of meshing, the *"skin element"* can be incorporated to the set of standard finite elements as a region of enhanced finite elements (see Fig. 2).

2.2 Variational formulation

For the purposes of this work, we shall now consider delamination phenomenon as a bidimensional mechanism represented by a 2D linear elastic model, composed by a potentially

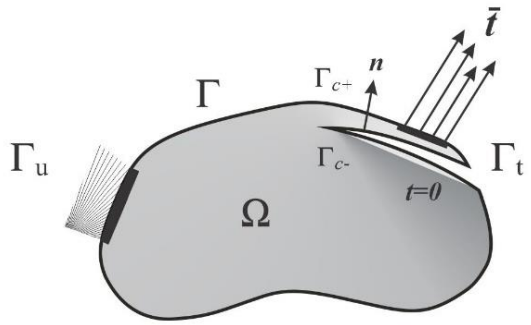

Fig. 3 Model of a solid-layer assembly subjected to traction forces on Γ_t inducing delamination effects over Γ_{c+} and Γ_{c-}

cracked domain Ω and the boundary Γ, which in turn can be decomposed in Γ_u (Dirichlet boundary conditions), Γ_t (Neumann boundary conditions) and Γ_c ($\Gamma_c = \Gamma_{c+} \cup \Gamma_{c-}$) (Cohesive boundary conditions). These boundary conditions must respect the Eq. (1)

$$\Gamma = \Gamma_u \cup \Gamma_t \cup \Gamma_{c+} \cup \Gamma_{c-} \text{ and } \Gamma_u \cap \Gamma_t \cap \Gamma_{c+} \cap \Gamma_{c-} = 0 \tag{1}$$

In this model, Γ_u is located at the non-cracked domain $\bar{\Omega}$, while Γ_t is placed over a pseudo-tissue, pulled away from the rest of the domain by a traction force applied over Γ_t. A known displacement value is imposed on Γ_u to guarantee the uniqueness of the displacement field (see Fig. 3). The crack tips are represented by Γ_{c+} and Γ_{c-}, which appear as soon as delamination phenomenon starts. In order to solve the boundary-value problem we will use the following equilibrium equations

$$\nabla \cdot \sigma + \mathrm{b} = 0 \tag{2}$$

$$\varepsilon = \varepsilon(\mathrm{u}) = \nabla_s \mathrm{u} \tag{3}$$

$$\sigma = \mathrm{C}{:}\,\varepsilon \tag{4}$$

In the last set of equations, the balance between internal and external forces is represented by equation Eq. (2), where σ is the Cauchy stress tensor, u corresponds to the displacement field, b are the body forces and n is the boundary normal unitary vector. Eq. (3) refers to the kinematic relationship between the displacement field $u(x)$ and the strain field $\epsilon(x)$, while the last Eq. (4) represents the constitutive behavior law for a homogeneous isotropic elastic material (assumed as the only one for all of the components), where $\nabla_s(\cdot)$ is the gradient operator's symmetric part and C is Hooke's fourth-order tensor. By combining Eqs. (3) and (4) with (2), we can solve the boundary-value problem of linear elasto-statics with or without delamination (Ibrahimbegovic 2010). Finally, we can apply the following boundary conditions for the problem without delamination

$$u = \bar{u} \qquad \text{over} \qquad \Gamma_u \tag{5}$$

$$\sigma \cdot n = \bar{t} \qquad \text{over} \qquad \Gamma_t \tag{6}$$

As soon as delamination phenomenon starts, we can assume that crack surfaces have no traction, so the following boundary conditions can be added for the decohesion zone

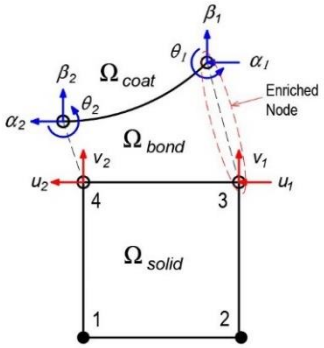

Fig. 4 Internal composition of the solid-layer element including three subdomains (solid, bonding and coat) with the nodal distribution of Degrees-Of-Freedom

$$\sigma \cdot n = 0 \qquad \text{over} \qquad \Gamma_{c+} \tag{7}$$

$$\sigma \cdot n = 0 \qquad \text{over} \qquad \Gamma_{c-} \tag{8}$$

3. Numerical implementation of the 2D solid-layer element

3.1 Numerical development based on a shape function's enhancement

For our purpose, the solid-layer element can be understood as a 2D enhanced-finite-element whose domain can be expressed as the assembling of three distinct sub-domains

$$\Omega^e = \Omega_{solid} \cup \Omega_{bond} \cup \Omega_{coat} \tag{9}$$

where Ω^e is the enhanced-finite-element domain, Ω_{solid} is the solid domain, Ω_{bond} is the bonding or interface domain, and Ω_{coat} corresponds the coat domain. In terms of the global finite element formulation, the set of the standard shape functions corresponding to the classical elements are enhanced with the supplementary shape functions of the solid-layer element, as it is expressed in Eq. (10)

$$u^h(x) = \sum_{I \in \mathcal{N}} N_I(x) u_I + \sum_{J \in \mathcal{N}^{skin}} \overline{N_J}(x) a_J \tag{10}$$

where $\mathcal{N}$ is the set of all standard nodes with classical continuum approximation and $\mathcal{N}^{skin}$ is the set of enhanced nodes with special functions associated to the solid-layer element. In other words, the 2D solid-layer element is based on the union of a classical four-nodes quadrilateral element with two translational Degree-Of-Freedom in each node; a two-node Bernoulli beam element with three Degree-Of-Freedom in each node (two translational DOF and one rotational DOF); and a pseudo four-nodes interface element, coupling the beam nodes to the solid nodes as it is shown in Fig. 4. The enhanced element will have a total of 14 DOF, with their respective number of integration points for each sub-domain (Dominguez 2005).

The formulation of the displacement field of the enriched solid-layer element can be written as follows

$$\mathbf{u}^h(\mathrm{x}) = \sum_{\mathrm{i}=1}^{4} N_i^{Solid}(\mathrm{x}) \cdot \mathbf{u}_i + \left[\sum_{\mathrm{i}=1}^{2} N_i^{Bond}(x) \cdot \mathbf{u}_i + \sum_{\mathrm{i}=3}^{4} N_i^{Bond}(x) \cdot \alpha_{\mathrm{i}} \right] + \sum_{i=1}^{2} N_i^{Coat}(x) \cdot \alpha_i \tag{11}$$

In the last expression, $\mathbf{u}_i$ is the set of nodal displacements associated to the continuous part of the solid elements, while α_i corresponds to the set of degrees of freedom belonging to the coating, representing the total displacement of the *skin* when this one is liberated. On the other hand, N_i^{Solid} are the standard bilinear shape functions for the domain Ω_{solid}; N_i^{Bond} are the special shape functions for the domain Ω_{bond}; and N_i^{Coat} are the standard Hermite shape functions for the domain Ω_{coat}.

3.2 Description of the shape functions

The construction of the shape functions is done for each sub-domain on the space of the natural coordinates, being independents between each one. For the solid body with two DOF's for node, we use the classical shape functions for a standard four-node quadrilateral element shown in Eqs. (12a)-(12d) (Hughes1987)

$$\mathrm{N}_1^s = \frac{1}{4} \cdot (1-\xi) \cdot (1-\eta) \tag{12a}$$

$$\mathrm{N}_2^s = \frac{1}{4} \cdot (1+\xi) \cdot (1-\eta) \tag{12b}$$

$$\mathrm{N}_3^s = \frac{1}{4} \cdot (1+\xi) \cdot (1+\eta) \tag{12c}$$

$$\mathrm{N}_4^s = \frac{1}{4} \cdot (1-\xi) \cdot (1+\eta) \tag{12d}$$

For the coat, which is modeled as a beam element with three DOF per node, the shape functions are formulated as follows: the translational displacements u_1 (projected on axis $x(\xi)$) are interpolated using the classical Lagrangian polynomial; on the other hand, the translational displacements u_2 (projected on axis $y(\eta)$) combined to the rotational displacements θ, are interpolated with the Hermite's polynomial using Eqs. (13) and (14)

$$\mathrm{v}^{\mathrm{e}}(\mathrm{x})[1 \quad \mathrm{x} \quad \mathrm{x}^2 \quad \mathrm{x}^3] * \begin{Bmatrix} \alpha_1 \\ \alpha_2 \\ \alpha_3 \\ \alpha_4 \end{Bmatrix} = F(x) \tag{13}$$

$$\theta^e(x) \simeq \frac{dv^e(x)}{dx} = [0 \quad 1 \quad 2x \quad 3x^2] * \begin{Bmatrix} \alpha_1 \\ \alpha_2 \\ \alpha_3 \\ \alpha_4 \end{Bmatrix} \tag{14}$$

The final Hermitian cubic shape functions are summarized in the set of Eqs. (15a)-(15f) with

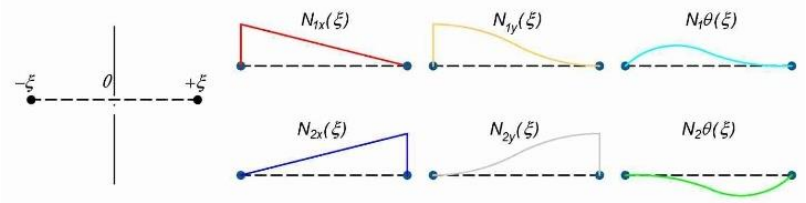

Fig. 5 First Order Lagrangian and Third Order Hermitian shape functions

the corresponding curves indicated in Fig. 5.

$$N_{1ux}^{b} = \frac{1}{2}\cdot(1 - \xi)\cdot(\eta) \tag{15a}$$

$$N_{1uy}^{b} = \frac{1}{4}\cdot(2 + 3\xi - \xi^3)\cdot(\eta) \tag{15b}$$

$$N_{1u\theta}^{b} = \frac{1}{4}\cdot(-1 - \xi + \xi^2 + \xi^3)\cdot(\eta) \tag{15c}$$

$$N_{2ux}^{b} = \frac{1}{2}\cdot(1 + \xi)\cdot(\eta) \tag{15d}$$

$$N_{2uy}^{b} = \frac{1}{4}\cdot(2 - 3\xi + \xi^3)\cdot(\eta) \tag{15e}$$

$$N_{2u\theta}^{b} = \frac{1}{4}\cdot(1 - \xi - \xi^2 + \xi^3)\cdot(\eta) \tag{15f}$$

Concerning to the bonding region, this one is formulated as a very thin four-node quadrilateral element where three linear sides are combined with a curved side connected to the coat: this side will reproduce the displacement and rotation's coat. The three sides are interpolated by using classical Lagrangian shape functions, while the curved side is interpolated with the same Hermitian cubic shape functions developed previously. The two nodes attached to the solid body conserve two DOF per node, while the nodes attached to the coat will have three DOF per node, in order to ensure the compatibility between the solid body and the coat. In other words, combining the shape functions of Eqs. (12) with Eqs. (15), we obtain a set of six shape functions (see Fig. 6) as it is shown in Eqs. (16a)-(16f) considering 10 DOF's (see Fig. 7).

$$N_{1}^{b} = \frac{1}{4}\cdot(1 - \xi)\cdot(1 - \eta) \tag{16a}$$

$$N_{2}^{b} = \frac{1}{4}\cdot(1 + \xi)\cdot(1 - \eta) \tag{16b}$$

$$N_{3u}^{b} = \frac{1}{8}\cdot(2 + 3\xi - \xi^3)\cdot(1 + \eta) \tag{16c}$$

$$N_{3\theta}^{b} = \frac{1}{8}\cdot(-1 - \xi + \xi^2 + \xi^3)\cdot(1 + \eta) \tag{16d}$$

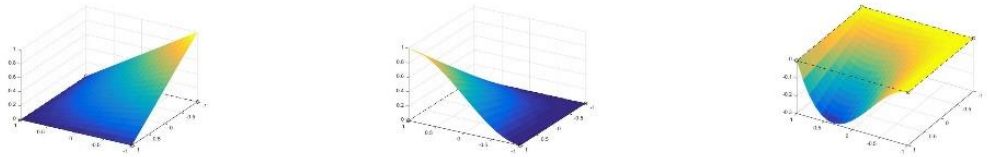

(a) Node 1 (b) Node 3 (c) Node 3θ

(d) Node 2 (e) Node 4 (f) Node 4θ

Fig. 6 Graphic representation of translational and rotational shape functions for bonding

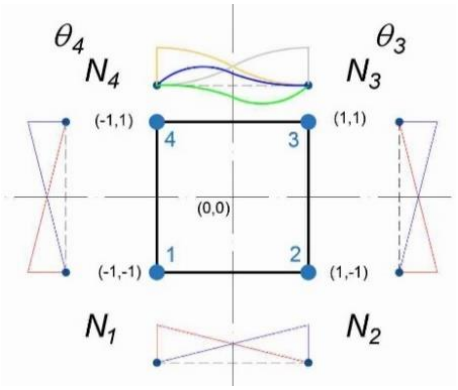

Fig. 7 Shape Functions for the Lagrangian-Hermitian bond interface

$$N_{4u}^{b} = \frac{1}{8} \cdot (2 - 3\xi + \xi^3) \cdot (1 + \eta) \tag{16e}$$

$$N_{4\theta}^{b} = \frac{1}{8} \cdot (1 - \xi - \xi^2 + \xi^3) \cdot (1 + \eta) \tag{16f}$$

3.3 Construction of the solid-layer stiffness matrix

In comparison to the classical 8×8 stiffness matrix of a standard QUAD4 element (see Fig. 8(a)), the stiffness matrix of the solid-layer element is the result of assembling three elementary arrays: the standard array of a QUAD4 element, the Hermitian array of a 2-node beam, and the special local matrix of bonding. This array must include the coupling between the translational DOF of the solid and the translational/rotational DOF of the coat. Considering that α_i, β_i and θ_i conform the set of enhanced DOF describing coat's free configuration, it is possible to build a 14×14 stiffness matrix for the whole solid-layer element as it is shown in Fig. 8(b).

In order to ensure the compatibility between the rigid body (solid) and the flexible layer (coat), it was necessary to develop a special array in which the Lagrangian shape functions are coupled to

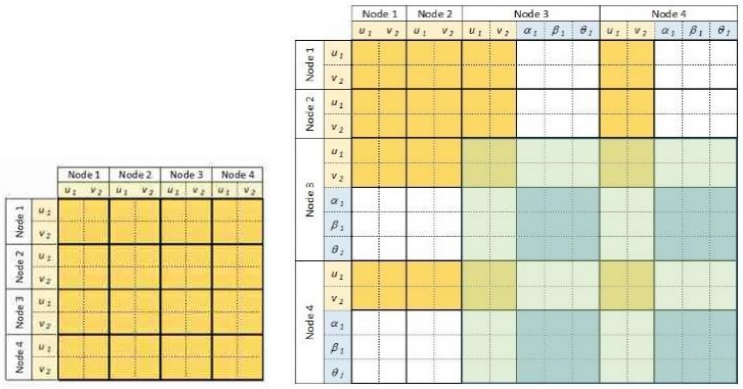

Fig. 8 Comparison between a standard 8×8 stiffness matrix for a QUAD4 element and the enhanced 14×14 stiffness matrix for the solid-layer element

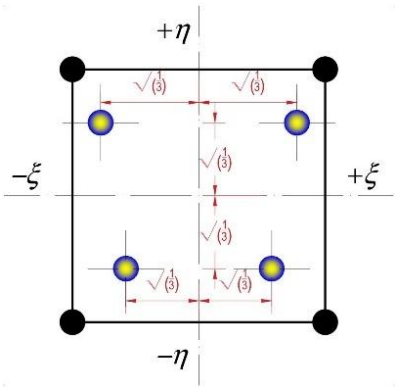

Fig. 9 Integration Gauss points in reference axis ξ and η

the Hermitian functions, using the set of shape functions indicated in Eq. (16).

3.4 Number and location of the integration points for the solid-layer element

Concerning to the numerical integration of the solid-layer element, each domain will have its own set of integration points in a similar way as it is done in (Dominguez *et al.* 2010). In other words, a 2×2 Gauss quadrature is implemented for the solid body, while a two integration points' array is adopted for the coat. Regarding to the bond region, a similar 2×2 Gauss quadrature array is adopted, being noteworthy that two integration points -those located near to the coat- are slightly relocated towards their closest nodes, due to the redistribution of energy induced by Hermitian shape functions (see Fig. 9).

3.5 Decohesion yield criterion based on a strain function

As explained throughout this document, cohesion's integrity is one of the most important key-points in the control of the combined behaviour of reinforced concrete and coat; nevertheless it could be damaged or deteriorated over time. For this reason, different non-linear models have been

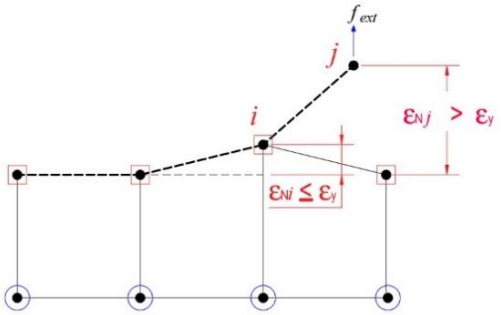

Fig. 10 Rigid Cohesion (RC) vs. Full Decohesion (FD): Node N_i is still attached to the concrete body, while Node N_j is fully separated

developed to simulate gradual decohesion, some of them based on Damage Mechanics or Fracture Mechanics (Turon *et al.* 2006, Ciavarella *et al.* 2008). Nevertheless, these approaches can be very complex to implement into our very first finite element proposal so we will adopt a simple criterion to determine two states of cohesion: Rigid Cohesion (RC)/Full Decohesion (FD). Likewise, instead of using a jump criteria based on absolute displacements (Camanho *et al.* 2008), we will use a simple criterion based on a strain yield function. In other words, when the bonding reaches certain normal strain on the perpendicular direction to the coat's surface, the coat will detach from the solid body. The decohesion strain function can be formulated as follows

$$\phi(\varepsilon)_{decohesion} = \langle \varepsilon^{bond} \rangle - \varepsilon_y \tag{17}$$

where $\phi(\varepsilon)_{decohesion}$is the decohesion function, $\langle \varepsilon^{bond} \rangle$ is the normal traction strain evaluated on each bonded node (only if it is positive), while ε_y is a decohesion strain yield constant. Therefore, the decohesion criterion evaluated on each bonded node can be stated as

$$Cohesion\ State \begin{cases} RC & \text{if } \phi(\varepsilon)_{decohesion} \leq 0 \\ FD & if \quad \phi(\varepsilon)_{decohesion} > 0 \end{cases}$$

In the last expression, only when $\phi(\varepsilon)_{decohesion}$ exceeds zero, the coat will be fully detached from the concrete body. Fig. 10 describes very well this criterion: while the bonded node N_i has not exceeded the strain limit, the bonded node N_j has already been detached from the mesh and the coat moves freely with wide rotations.

4. Numerical validation

4.1 Testing and validation of bonding formulation

The core of the solid-layer element is the bonding formulation. In order to perform a numerical validation, two patch tests will be implemented for the bonding, formulated solely as a single element: (a) in the first test, a traction force will be applied along the coat (see Fig. 11(a)); (b) in the second test, a bending moment will be applied on one coat's edge (see Fig. 11(b)). The aim of both tests is to ensure that bonding transition reproduces simultaneously the combined translational displacement of coat and concrete, when they are fully attached. The tests are

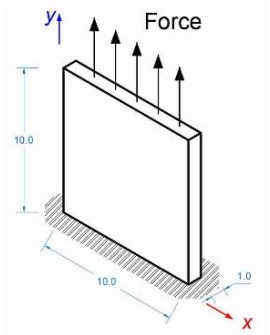

(a) Axial force on y

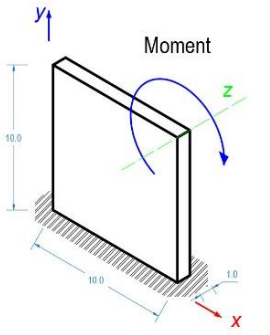

(b) Bending moment around z

Fig. 11 Numerical validation of the solid-layer bonding transition through the implementation of two patch-tests

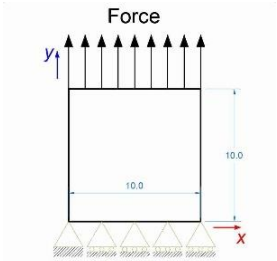

(a) Traction force applied on y direction (variant A)

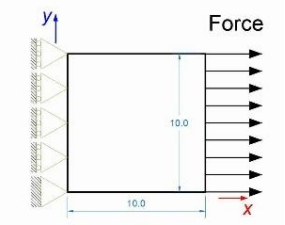

(b) Traction force applied on x direction (variant B)

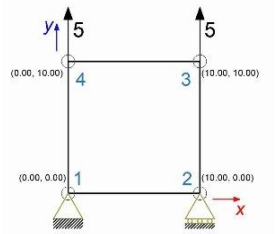

(c) Concentrated traction force on y direction (variant A)

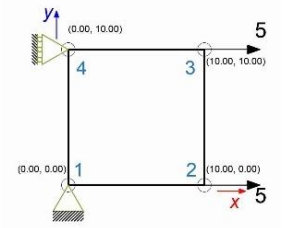

(d) Concentrated traction force on x direction (variant B)

Fig. 12 Traction test on a 2D solid-layer bonding element, two variants: (A) vertical loading; (B) horizontal loading

performed as it is shown in Fig. 11, with the following properties: Young's modulus $E = 1000.0\,\mathrm{N/cm^2}$, Poisson's ratio $\nu = 0.10$, thickness $t = 1.0$ cm, length $l = 10.0$ cm, height $h = 10.0$ cm. In both tests, the coat is placed on the upper side of the single element.

4.1.1 Traction test

In this test a distributed traction load of 10.0 N will be applied along one side of the single element; meanwhile, the opposite side is partially restrained to reproduce a homogeneous state of traction stress in the whole element. By the way, the traction test has two variants: in the first one, the traction force is placed on the upper side of the element (where the coat is attached), while the

Table 1 Nodal displacements obtained on the Traction Test

Node	Variant A: Force on *x* axis			Variant B: Force on *y* axis		
	u_x	u_y	θ_z	u_x	u_y	θ_z
1	0.000	0.000	- -	0.000	0.000	- -
2	-0.001	0.000	- -	0.010	0.000	- -
3	-0.001	0.010	0.000	0.010	-0.001	0.000
4	0.000	0.010	0.000	0.000	-0.001	0.000

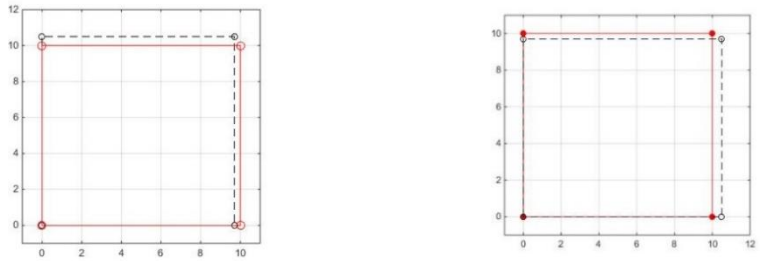

(a) Displacement on *x* (b) Displacement on *y*

Fig. 13 Numerical validation of the solid-layer bonding transition through the implementation of two patch-tests

lower side is partially restrained as it is shown in Fig. 12(a). In the second variant, the traction load is applied on the element's right side, while the left side is partially restrained as indicated in Fig. 12(b): the coat remains attached to the upper side for the element. Both tests are solved analytically using a plane stress assumption, obtaining similar results:

• Traction load on *Y* direction:

$$\sigma_y = 1.0\,\mathrm{N/cm^2},\ \epsilon_x = -0.0001,\ \epsilon_y = 0.001$$

• Traction load on *X* direction:

$$\sigma_x = 1.0\,\mathrm{N/cm^2},\ \epsilon_x = 0.001,\ \epsilon_y = -0.0001$$

The two variants of the traction test will be solved numerically as a 2D plane stress problem, using a special Hermite-Lagrangian Quad4 element with 10 DOF: two translational DOF on nodes 1 to 4, and one extra-rotational DOF on nodes 3 and 4 (see Figs. 12 (c)-(d)). As a consequence, the system of linear equations can be set up as follows

$$\{\mathbf{u}\}_{(10\times1)} = [\mathbf{K}]^{-1}_{(10\times10)} \cdot \{\mathbf{f}_{ext}\}_{(10\times1)} \tag{18}$$

Accordingly, in order to include the effects of any external bending moment into the bond element nodes, it will be necessary to enhance the standard force array of 8×1 to a vector of 10×1 in the following manner

$$\mathbf{f}_{ext} = [f_{x1} \quad f_{y1} \quad f_{x2} \quad f_{y2} \quad f_{x3} \quad f_{y3} \quad \boldsymbol{m_{z3}} \quad f_{x4} \quad f_{y4} \quad \boldsymbol{m_{\theta 4}}] \tag{19}$$

The set of nodal displacements obtained by solving the matrix equation for the two variants of the traction test, is shown in Table 1.

Likewise, the set of strains and stresses obtained at the first integration point for variant B is shown in the vectors (see Eq. (20)). It is important to highlight the change of position of some integration points as a consequence of the higher-dimensional integration associated to the special

Table 2 Nodal displacements obtained on the Moment Test

Node	Positive Moment			Negative Moment		
	u_x	u_y	θ_z	u_x	u_y	θ_z
1	0.0000	0.000	- -	0.0000	0.0000	- -
2	-0.0104	0.000	- -	0.0104	0.0000	- -
3	-0.0010	0.0001	0.0979	0.0010	-0.0001	0.0
4	-0.0094	-0.0001	-0.0934	0.0094	0.0001	0.000

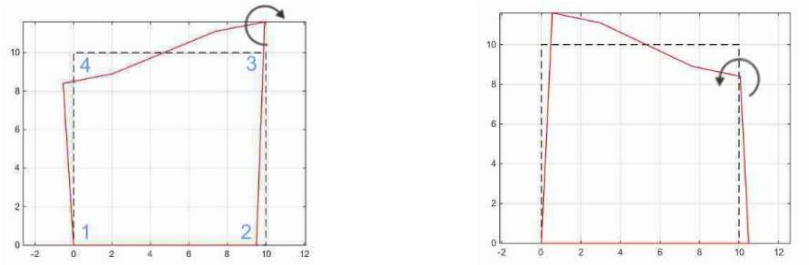

(a) Displacement by (+) spin (b) Displacement by (-) spin

Fig. 14 Displacement field for the two variants of the bending moment test on bond formulation

Hermite shape functions known as Hermite cubature (as it was shown in Fig. 9). In any case, the numerical results are identical to the analytical solution of the two variants of the traction test.

$$\boldsymbol{\epsilon_{pg1}} = \begin{bmatrix} -0.0001 \\ 0.001 \\ 0.0000 \end{bmatrix} \qquad \boldsymbol{\sigma} = \begin{bmatrix} -0.10 \\ \mathbf{1.00} \\ 0.00 \end{bmatrix} \tag{20}$$

Finally, the deformed configuration of both variants (A and B) of the traction test are shown in Fig. 13.

4.1.2 Bending moment test

One of the main purposes of the bond formulation is the ability to impose bending moments on one of the faces and reproduce any rotation; by applying a unitary bending moment on one of the nodes where the coat is attached, we will be able to obtain translational displacements on x and y axis as well as the θ spin on these nodes. In order to verify it, a unitary bending moment will be applied on node 3, with two variants: in the first one, the moment turns clockwise, while in the second one it turns in anti-clockwise direction, as it is shown in their respective external force's vector (see vectors on Eq. (21)).

$$\begin{aligned} \mathbf{f}_{ext} &= [0 \quad 0 \quad 0 \quad 0 \quad 0 \quad 0 \quad \mathbf{+1} \quad 0 \quad 0 \quad \mathbf{0}] \text{ clockwise moment} \\ \mathbf{f}_{ext} &= [0 \quad 0 \quad 0 \quad 0 \quad 0 \quad 0 \quad \mathbf{-1} \quad 0 \quad 0 \quad \mathbf{0}] \quad \text{anti-clockwise moment} \end{aligned} \tag{21}$$

In order to solve this problem, we will reuse the matrix Eq. (18). The nodal displacements (including translational and rotational displacements) induced by the two variants: the clockwise (positive) moment and the anti-clockwise (negative) moment, are summarized in Table 2.

The deformed configuration of both variants (clockwise and anti-clockwise moments) is shown in Fig. 14.

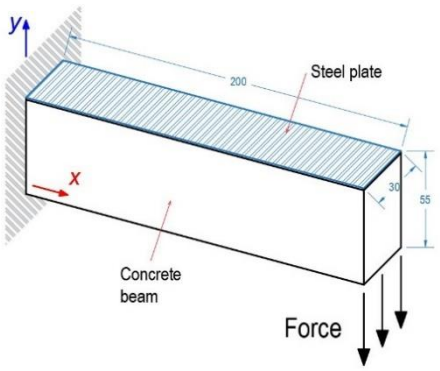

Fig. 15 Modelling of a cantilever beam with a concentrated force on the edge

4.2 Testing the skin element: the assemblage of solid, bonding and coat

In this study, we present on a simple cantilever beam. A similar numerical test was performed by (Tahar *et al.* 2021) but instead of simulating one phase, we studied the development of the three phases of coat's detachment: phase 1 corresponds to perfect bonding; phase 2 represents the partial debonding at yield point; and phase 3 reproduces total debonding of the skin element. For that purpose, a cantilever concrete beam with elastic behavior is modelled as it is shown in the Fig. 15.

For this test, the following material and geometrical characteristics were used: for concrete body, an elasticity modulus $E = 2.2 \times 10^4$ MPa and a Poisson ratio $\nu = 0.10$ with a transversal section of 30×55 cm; for the steel plate, an elasticity modulus $E = 2.0 \times 10^5$ MPa and thickness $e = 1.3$ cm. The length of the beam is 200 cm.

The analytical solution of this problem gives the following results: the failure of the unreinforced concrete occurs when the allowable ultimate load reaches a value of 23,821.80 N, inducing a vertical deflection of $\delta = 0.069$ cm; eventually, the load is increased to reach a positive strain criterion of $\varepsilon = 0.001$ on the nodes of coat/bond, indicating the end of the phase 1, starting phases 2 and 3 of debonding. By the way, in order to test the effectiveness of the solid-layer element, we built two kind of meshes: the mesh shown in Fig. 16(a) consists in a set of four standard QUAD4 elements attached to 4 solid-layer elements, while the second mesh shown in Fig. 16(b) consists in a mixed mesh of 8 standard QUAD4 elements with 8 solid-layer elements.

For our purposes, four cases are studied and compared for the numerical test:

- Unreinforced concrete beam solved analytically;
- Unreinforced concrete beam solved with Lag-Her Q4 elements;
- Plate reinforced concrete beam solved with Lag-Her Q4 elements
- Plate reinforced concrete beam solved with Lag-Her Q4 elements and debonding activation;

The aim of the first case is to deduce the maximum displacement at the edge of the cantilever beam using an analytical solution, to use it as a reference. At the same time, it allows to evaluate the elastic stiffness of the plane concrete beam without reinforcement. The second case tries to reproduce the analytical results using a standard mesh analyzed with the Finite Element Method. As attended, the FEM analysis shows a stiffer beam's capacity, even if the second curve is very close to the first case's curve. The third case represents a classical FEM simulation where the reinforcement or over coat is attached to the beam's top face, without any possibility of decohesion: in this case, the stiffness of the combined beam (over coat and concrete) is greater

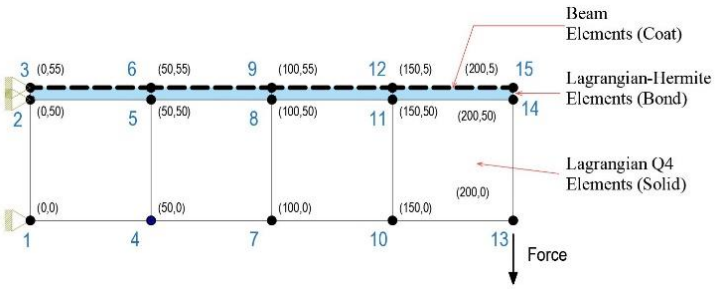

(a) Mesh type 1

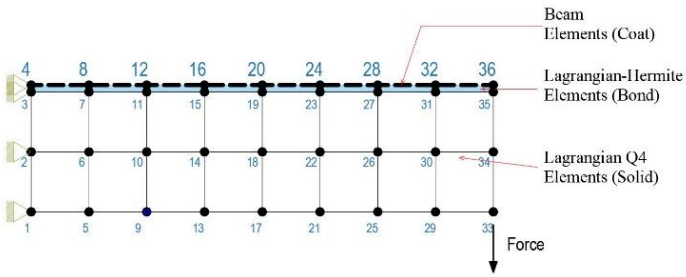

(b) Mesh type 2

Fig.16 FEM Cantilever Beam to test bond element

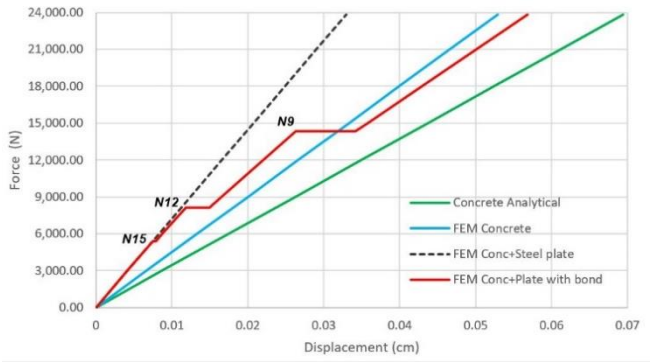

(a) Mesh type 1

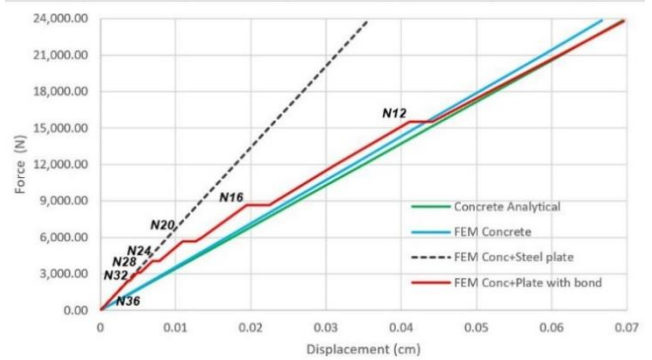

(b) Mesh type 2

Fig. 17 Comparison of the structural response of cantilever beam's four cases using meshes type 1 and 2

Table 3 Maximum displacement in cantilever beams

Case	Analytical	FEM Conc.	FEM C+P	FEM C+P+B
Mesh 1	0.06942	0.05289	0.03295	0.05658
Mesh 2	0.06942	0.06667	0.03556	0.06963

than unreinforced concrete beam's stiffness. In the third case (concrete beam reinforced with a covering steel plate), the maximum displacement diminishes, but this condition is only fulfilled if the perfect union between both materials is maintained.

The fourth case intends to reproduce the damage of the bonding between the coat and the concrete, with the progressive detachment between them. This phenomenon is represented in the beam applying a strain criterion based on the sliding between both surfaces (Dominguez *et al.* 2010). As soon as a yield decohesion criteria is surpassed in a node, the detachment starts. For this case, node 36 -which is in the edge of the beam- is the first node where decohesion occurs, reducing the stiffness of the beam in a certain proportion. As soon as detachment progresses in nodes 32, 28, 24, 20, 16 and 12, the capacity of the beam "*jumps*" and reduces its stiffness, reaching the capacity curve of the unreinforced concrete beam.

A comparison of the structural capacity of the four cases is shown in Fig. 17(a) when a coarse mesh is used (Mesh type 1); Fig. 17(b) shows the same structural capacity's comparison with a fine mesh (Mesh type 2). Meanwhile, the vertical displacements of the four cases obtained with both meshes are listed in Table 3.

5. Conclusions

The solid-layer element (or skin element) can be useful to describe the phenomenon of delamination between concrete and overcoating by reformulating in just one element the solid concrete body, the coat and the bonding zone, being able to reproduce the adhesive interface matrix that joins them. Adopting a strain criteria for debonding, it is possible to fully describe phases 1, 2, 3 and 4 of the delamination process. Another aspect of the solid-layer element to highlight is its ability to reproduce rotations on one face of a solid element. The solid-layer element allows us to calculate not only the translational displacements, but also the spin and curvature on one side of the element, caused by external forces/moments solicitations. Namely, this proposal aims to provide of a special finite element which serves as an interface between a solid with small deformations and a skin with large rotations.

The extension of this work to dynamics can be accomplished by following the recent ideas presented in references (Mejia-Nava *et al.* 2021, Ibrahimbegovic and Mejia-Nava 2021).

Acknowledgements

The authors gratefully acknowledge the financial support of CONACYT (Consejo Nacional de Ciencia y Tecnología of Mexico) which funded the project PDPN/2015-1187 as well as the Arturo Suarez Suarez's doctoral scholarship.

References

Abderezak, R., Daouadji, T.H. and Rabia, B. (2020), "Analysis of interfacial stresses of the reinforced concrete foundation beams repairing with composite materials plate", *Couple. Syst. Mech.*, **9**(5), 473-498. https://doi.org/10.12989/csm.2020.9.5.473.

Abderezak, R., Daouadji, T.H. and Rabia, B. (2021), "Fiber reinforced polymer in civil engineering: Shear lag effect on damaged RC cantilever beams bonded by prestressed plate", *Couple. Syst. Mech.*, **10**(4), 299-316. https://doi.org/10.12989/csm.2021.10.4.299.

Akbas, S.D. (2019), "Forced vibration analysis of functionally graded sandwich deep beams", *Couple. Syst. Mech.*, **8**(3), 259-271. https://doi.org/10.12989/csm.2019.8.3.259.

Akbas, S.D. (2020), "Dynamic analysis of a laminated composite beam under harmonic load", *Couple. Syst. Mech.*, **9**(6), 563-573. https://doi.org/10.12989/csm.2020.9.6.563.

Al-Osta, M.A. (2019), "Shear behaviour of RC beams retrofitted using UHPFRC panels epoxied to the sides", *Comput. Concrete*, **24**(1), 37-49. https://doi.org/10.12989/cac.2019.24.1.037.

Andrews, G.E., Askey, R. and Roy, R. (1987), *Encyclopedia of Mathematics and its Applications; Special Functions*, Cambridge University Press, Cambridge, U.K.

Bideci, A., Bideci, Ö.S., Oymael, S., Gültekin, A.H. and Yıldırım, H. (2017), "Lightweight aggregates coated with colemanite", *Comput. Concrete*, **19**(5), 451-455. https://doi.org/10.12989/cac.2017.19.5.451.

Camanho, P.P., Turon, A. and Costa, J. (2008), "17-Delamination propagation under cyclic loading", *Delamination Behaviour of Composites*, Woodhead Publishing Series in Composites Science and Engineering, 485-513.

Ciavarella, M., Paggi, M. and Carpinteri, A. (2008), "One, no one, and one hundred thousand crack propagation laws: A generalized Barenblatt and Botvina dimensional analysis approach to fatigue crack growth", *J. Mech. Phys. Solid.*, **56**(12), 3416-3432. https://doi.org/10.1016/j.jmps.2008.09.002.

Cimellaro, G.P. (2013), "11-Resilience-based design (RBD) modelling of civil infrastructure to assess seismic hazards", *Handbook of Seismic Risk Analysis and Management of Civil Infrastructure Systems*, **91**, 268-303.

Daouadji, T.H. (2017), "Analytical and numerical modeling of interfacial stresses in beams bonded with a thin plate", *Adv. Comput. Des.*, **2**(1), 57-69. https://doi.org/10.12989/acd.2017.2.1.057.

De Borst, R. and Remmers, J.C. (2006), "Computational modelling of delamination", *Compos. Sci. Technol.*, **66**(6), 713-722.

Ding, W. (1999), "Delamination analysis of composite laminates", Ph.D. Dissertation, University of Toronto, Canada.

Dolbow, J. (1999), "An extended finite element method with discontinuous enrichment for applied mechanics", Ph.D. Dissertation, Northwestern University, Evanston, IL., USA.

Dominguez, N. (2005), "Étude de la liaison acier-béton: de la modélisation du phénomène à la formulation d'un élément fini enrichi Béton Armé", Ph.D. Dissertation, École Normale Supérieure de Cachan, France.

Dominguez, N. and Ibrahimbegovic, A. (2012), "A non-linear thermodynamical model for steel-concrete bonding", *Comput. Struct.*, **29**(45), 29-45. https://doi.org/10.1016/j.compstruc.2012.04.005.

Dominguez, N., Fernandez, M.A. and Ibrahimbegovic, A. (2010), "Enhanced solid element for modelling of reinforced concrete structures with bond-slip", *Comput. Concrete*, **7**(4), 347-364. https://doi.org/10.12989/cac.2010.7.4.347.

Ebadi-Jamkhaneh, M., Homaioon-Ebrahimi, A. and Kontoni, D.P.N. (2021), "Numerical finite element study of strengthening of damaged reinforced concrete members with carbon and glass FRP wraps", *Comput. Concrete*, **28**(2), 137-147. https://doi.org/10.12989/cac.2021.28.2.137.

Gobierno, del D.F. (2017), "Normas técnicas complementarias para el diseño y construcción de estructuras de acero", *Reglamento de Construcciones del Distrito Federal*, Ciudad de México, México.

Hossain, K.M. and Olufemi, O.O. (2004), "Computational optimisation of a concrete model to simulate membrane action in RC slabs", *Comput. Concrete*, **1**(3), 325-354. https://doi.org/10.12989/cac.2004.1.3.325.

Hughes, T.J.R. (1987), *The Finite Element Method. Linear Static and Dynamic Finite Element Analysis*, Prentice-Hall International Editions, New Jersey, USA.

Ibrahimbegovic, A. (2010), *Nonlinear Solid Mechanics: Theoretical Formulations and Finite Element Solution Methods*, Springer, Dordrecht, Heidelberg, London, New York.

Ibrahimbegovic, A. and Nava, R.A.M. (2021), "Heterogeneities and material-scales providing physically-based damping to replace Rayleigh damping for any structure size", *Couple. Syst. Mech.*, **10**(3) 201-216, https://doi.org/10.12989/csm.2021.10.3.201.

Iglesias, J., Robles, F.V., De la Cera, J.A. and González, O. (1985), "Reparación de estructuras de concreto y mampostería", Departamento de Ciencias e Ingeniería, UAM, Ciudad de México, México.

Kim, S.H. and Aboutaha, R.S. (2004), "Finite element analysis of carbon fiber-reinforced polymer (CFRP) strengthened reinforced concrete beams", *Comput. Concrete*, **1**(4), 401-416. https://doi.org/10.12989/cac.2004.1.4.401.

Lee, C., Bonacci, J.F. and Thomas, M.D.A. (2000), "Accelerated corrosion and repair of reinforced concrete columns using carbon fiber reinforced polymer sheets", *Can. J. Civil Eng.*, **211**, 941-948. https://doi.org/10.1139/l00-030.

Limaiem, M., Ghorbel, E. and Limam, O. (2019), "Comparative experimental study of concrete reparation with carbon epoxy & bio-resourced composites", *Constr. Build. Mater.*, **201**, 312-323. https://doi.org/10.1016/j.conbuildmat.2019.03.137.

MacGregor, J.G., Wight, J.K., Teng, S. and Irawan, P. (1997), *Reinforced Concrete: Mechanics and Design*, Prentice Hall Upper Saddle River, NJ, U.S.A.

Matthew, D.J. and Mehrdad, S. (2020), "Building performance for earthquake resilience", *Eng. Struct.*, **210**, 110371. https://doi.org/10.1016/j.engstruct.2020.110371.

Mejia-Nava, R.A., Ibrahimbegovic, A., Domínguez-Ramírez, N. and Flores-Mendez, E. (2021), "Viscoelastic behavior of concrete structures subject to earthquake", *Couple. Syst. Mech.*, **10**(3) 263-280, https://doi.org/10.12989/csm.2021.10.3.263.

Melenk, J.M. and Babuska, I. (1996), "The partition of unity finite element method: Basic theory and applications", *Comput. Meth. Appl. Mech. Eng.*, **139**(1-4), 289-314. https://doi.org/10.1016/S0045-7825(96)01087-0.

Moes, N., Dolbow, J. and Belytschko, T. (2012), "A finite element method for crack growth without remeshing", *Int. J. Numer. Meth. Eng.*, **46**(1), 131-150. https://doi.org/10.1002/(SICI)1097-0207(19990910)46:1<131::AID-NME726>3.0.CO;2-J.

Mohebi, B., Hosseinifard, S.M. and Bastami, M. (2016), "Plastic hinge characteristics of RC rectangular columns with Fiber Reinforced Polymer (FRP)", *Comput. Concrete*, **18**(4), 853-876. https://doi.org/10.12989/cac.2016.18.4.853.

Nasser, H., Van-Steen, Ch., Vandewalle, L. and Verstrynge, E. (2021), "An experimental assessment of corrosion damage and bending capacity reduction of singly reinforced concrete beams subjected to accelerated corrosion", *Constr. Build. Mater.*, **286**, 122773. https://doi.org/10.1016/j.conbuildmat.2021.122773.

Park, J.G., Lee, K.M., Shin, H.M. and Park, Y.J. (2007), "Nonlinear analysis of RC beams strengthened by externally bonded plates", *Comput. Concrete*, **4**(2), 119-134. https://doi.org/10.12989/cac.2007.4.2.119.

Rezaiee-Pajand, M. and Karimipour, A. (2020), "Two rectangular elements based on analytical functions", *Adv. Comput. Des.*, **5**(2), 147-175. https://doi.org/10.12989/acd.2020.5.2.147.

Shaw, I.D. and Andrawes, B. (2017), "Finite element analysis of CFRP laminate repairs on damaged end regions of prestressed concrete bridge girders", *Adv. Comput. Des.*, **1**(2), 147-168. https://doi.org/10.12989/acd.2017.1.2.147.

Siu, W.H. and Su, R.K.L. (2011), "Analysis of side-plated reinforced concrete beams with partial interaction", *Comput. Concrete*, **8**(1), 71-96. https://doi.org/10.12989/cac.2011.8.1.071.

Sukumar, N. and Prévost, J.H. (2003), "Modeling quasi-static crack growth with the extended finite element method Part I: Computer implementation", *Int. J. Solid. Struct.*, **40**(26), 7513-7537. https://doi.org/10.1016/j.ijsolstr.2003.08.002.

Tahar, H.D., Abderezak, R. and Rabia, B. (2020), "Hyperstatic steel structure strengthened with prestressed

carbon/glass hybrid laminated plate", *Couple. Syst. Mech.*, **10**(5), 393-414. https://doi.org/10.12989/csm.2020.10.5.393.

Tahar, H.D., Abderezak, R., Rabia, B. and Tounsi, A. (2021), "Performance of damaged RC continuous beams strengthened by prestressed laminates plate: Impact of mechanical and thermal properties on interfacial stresse", *Couple. Syst. Mech.*, **10**(2), 161-184. https://doi.org/10.12989/csm.2021.10.2.161.

Turon, A., Camanho, P.P., Costa, J. and Dávila, C.G. (2006), "A damage model for the simulation of delamination in advanced composites under variable-mode loading", *Mech. Mater.*, **38**(11), 1072-1089. https://doi.org/10.1016/j.mechmat.2005.10.003.

Xiongfei, L. and Yue, L. (2018), "Experimental study of seismic behavior of partially corrosion-damaged reinforced concrete columns strengthened with FRP composites with large deformability", *Constr. Build. Mater.*, **191**, 1071-1081. https://doi.org/10.1016/j.conbuildmat.2018.10.072.

Xiongfei, L. and Yue, L. (2019), "Static bearing capacity of partially corrosion-damaged reinforced concrete structures strengthened with PET FRP composites", *Constr. Build. Mater.*, **211**, 33-43. https://doi.org/10.1016/j.conbuildmat.2019.03.218.

Yang, H., Song, H. and Zhang, S. (2015), "Experimental investigation of the behavior of aramid fiber reinforced polymer confined concrete subjected to high strain-rate compression", *Constr. Build. Mater.*, **95**, 143-151. https://doi.org/10.1016/j.conbuildmat.2015.07.084.

Zienkiewicz, O.C., Taylor, R.L. and Zhu, J.Z. (2006), *The Finite Element Method-It's Basis and Fundamentals*, Butterworth-Heinemann.